

Access to this work was provided by the University of Maryland, Baltimore County (UMBC) ScholarWorks@UMBC digital repository on the Maryland Shared Open Access (MD-SOAR) platform.

Please provide feedback

Please support the ScholarWorks@UMBC repository by emailing scholarworks-group@umbc.edu and telling us what having access to this work means to you and why it's important to you. Thank you.

A 3D-printed, modular, and parallelized microfluidic system with customizable scaffold integration to investigate the roles of basement membrane topography on endothelial cells

Curtis G. Jones¹, Tianjiao Huang², Jay H. Chung², and Chengpeng Chen^{1*}

1. Department of Chemistry and Biochemistry, University of Maryland Baltimore County, Baltimore, MD, USA, 21250

2. Laboratory of Obesity and Aging Research, Cardiovascular Branch, National Heart Lung and Blood Institute, Bethesda, MD, USA, 20892

*Correspond to Dr. Chengpeng Chen

cpchen@umbc.edu

410-455-3053

ABSTRACT

Because dysfunctions of endothelial cells are involved in many pathologies, *in vitro* endothelial cell models for pathophysiological and pharmaceutical studies have been a valuable research tool. Although numerous microfluidic-based endothelial models have been reported, they had the cells cultured on a flat surface without considering the possible 3D structure of the native ECM. Endothelial cells rest on the basement membrane *in vivo*, which contains an aligned microfibrinous topography. To better understand and model the cells, it is necessary to know if and how the fibrous topography can affect endothelial functions. With conventional fully integrated microfluidic apparatus, it is difficult to include additional topographies in a microchannel. Therefore, we developed a modular microfluidic system by 3D-printing and electrospinning, which enabled easy integration and switching of desired ECM topographies. Also, with standardized designs, the system allowed for high flow rates up to 4000 $\mu\text{L}/\text{min}$, which encompassed the full shear stress range for endothelial studies. We found that the aligned fibrous topography on the ECM altered arginine metabolism in endothelial cells, and thus increased nitric oxide production. There has not been an endothelial model like this, and the new knowledge generated thereby lays a groundwork for future endothelial research and modeling.

Keywords: 3D-printing, microfluidics, endothelial cells, scaffolds

INTRODUCTION

Endothelial cells exist in all organs as the inner-most layer of blood vessels and play critical roles in maintaining the homeostasis of the cardiovascular system and blood-tissue interfaces^{1, 2}. Endothelial dysfunctions are involved in a myriad of pathologies such as the complications from diabetes, cardiovascular diseases (CVD), and stroke³⁻⁶. Therefore, the ability to model endothelial cells *in vitro* for pathophysiological and pharmaceutical studies has been a valuable research tool. Compared to static models (e.g., in culture flasks), microfluidic-based endothelial models are more physiological because the media flow can continuously provide nutrients and remove metabolic wastes^{7, 8}. More importantly, microfluidics allows for the introduction of flow-based shear stress, which is known to mechanically couple blood-flow to endothelial function^{9, 10}. Although numerous microfluidic designs for endothelial studies have been reported in the past two decades, most of them applied a 2D extracellular matrix (ECM; e.g., a coated layer of collagen and/or fibronectin) for the cells, without considering the possible 3D structures of the native ECM¹¹⁻¹⁷. *In vivo*, endothelial cells rest on a 3D surface called the basement membrane (BM), which lines blood vessels¹⁸. As shown in **Fig. 1A**, Klee et al. reported the arterial BM contains an aligned fibrous topography along the blood flow direction¹⁹. We also sliced longitudinally decellularized human artery specimens, imaged them, and found similar topographies with microfibers of 1-3 μm thickness (**Fig. 1B**). A few studies reported that ECM microstructures (e.g., micropillars) might affect endothelial cell functions, but not on physiologically relevant topographies²⁰⁻²². To better understand endothelial cell biology and model the cells in the future, the effects of the aligned microfibrous surface of BM on the cell functions will need to be understood.

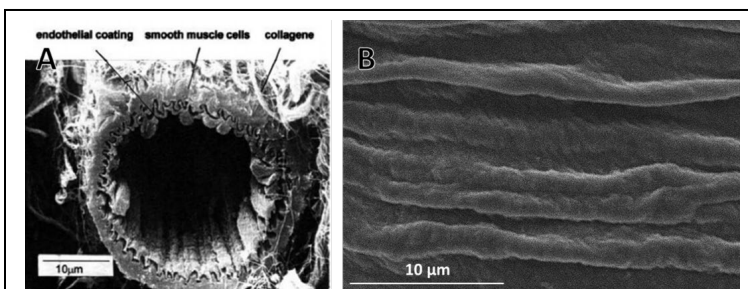


Figure 1. (A) A cross-sectional view of an artery showing that the basement membrane is not a flat matrix. Instead, a microfibrous topography can be seen along the blood vessel direction. Image reprinted from SpringerNature (license number 4942630469874). **(B)** A longitudinal view of the interior of a piece of decellularized human conduit artery. Various artery specimens were measured, and the diameter of the aligned fibers was found to be in the range of 1-3 μm .

To conduct such a study, it would be ideal to have a microfluidic device that enables simple integration and switching of various control ECM topographies (e.g., aligned fibrous and flat). However, such technology remains to be developed. In this paper, we present a new 3D-printed microfluidic system

that can satisfy these criteria. Specifically, modular ECMs were prepared in a high throughput manner, which could be simply integrated into a 3D-printed microfluidic device within seconds. The device was remarkably robust, enabling flow rates of 0-4000 $\mu\text{L}/\text{min}$ without leakage. These flow rates encompass the entire physiologically relevant shear stress (0-80 dyne/cm^2) range that is experienced by endothelial cells *in vivo*²³. In addition, this technology allowed for cell removal at any time to assess intracellular activities (e.g., metabolomics measurements). The device was also scaled up to run 12 experiments simultaneously. Facilitated by these unique features of the microfluidic setup, it was found that the aligned microfibrillar topography could significantly enhance the production of nitric oxide (NO), a critical functional molecule released from endothelial cells which can control vasodilation and platelet activation, etc²⁴⁻²⁸. Further targeted metabolomics measurements by liquid chromatography-mass spectrometry (LC-MS)²⁹ and enzyme activity probing confirmed the NO results.

EXPERIMENTAL

Materials and chemicals

Chemicals: tetrahydrofuran (THF, MilliporeSigma, MO, USA), dimethylformamide (DMF, MilliporeSigma, MO, USA), 70% (w/v) ethanol (Thermo Fisher Scientific, MA, USA), collagen (MilliporeSigma, MO, USA), DMEM media (Thermo Fisher Scientific, MA, USA), fetal bovine serum (FBS, MilliporeSigma, MO, USA), penicillin-streptomycin (Thermo Fisher Scientific, MA, USA), DAF-FM (MilliporeSigma, MO, USA), adenosine triphosphate (MilliporeSigma, MO, USA), crystal violet (VWR, PA, USA), ¹³C-phenylalanine (Cambridge Isotope Laboratories, Inc., MA, USA), LC-MS grade isopropanol (Millipore-Sigma, MO, USA), LC-MS grade water (Millipore-Sigma, MO, USA), LC-MS grade methanol (Fisher Scientific, Hampton, NH, USA), nitric oxide, compressed gas (Airgas, PA, USA)

Materials: polystyrene 192,000 MW (MilliporeSigma, MO, USA), polystyrene Sheets (Shrinky Dinks, MI, USA), Tygon tubing with ID 0.020" and OD 0.060" (Cole-Parmer, IL, USA), Ismatec Pump Tubing 0.64 mm ID (Cole-Parmer, IL, USA).

Electrospinning to fabricate the aligned microfibrillar topography

An electrospinning polymer solution was prepared by dissolving 4.0000g of 192,000 MW polystyrene in an organic mixture of 60%/40% (v/v) THF/DMF with a total volume of 10 mL. The resulting solution was then placed on an orbital shaker at 37 °C until homogenization. Then approximately 1mL of the polymer solution was loaded into a syringe affixed with a 20-gauge blunt needle (stainless steel) and placed in a syringe pump (New Era, NY, USA) of a custom-built electrospinning apparatus. A 10.16 x 6.35

cm sheet of polystyrene (250 μ m thick) was attached to a rotating mandrel inside of the electrospinning device, which was placed 20 cm from the tip of the needle. Then, a clamp connected to a power supply (Spellman High Voltage, model CZE1000R, NY, USA) was fastened to the blunt needle tip. A 15 x 15 cm copper plate was positioned 20 cm away from the rotating mandrel opposite the dispensing syringe. Two wires on both sides of the rotating mandrel were affixed to the grounded copper plate. Since the polystyrene sheet is not a conductive material, the copper plate functioned as a second grounding surface to direct the flow of generated fibers over the polystyrene surface. The mandrel was set to rotate at 4500 rpm, with which, the fibers were observed to orient in a uniform direction on the polystyrene sheet.

A flow rate of 1.5 mL/hr was applied to the syringe pump, and upon consistent flow through the needle tip, the power supply was turned on with a voltage of 22.5 kV. To ensure a uniform coating of the fibers across the polystyrene sheet, every 45 seconds, the mandrel was moved laterally by 1.25 cm for a total of 7 times. After the electrospinning, the polystyrene sheet covered with aligned fibers was removed for insert preparation.

Insert preparation

The fiber-coated polystyrene sheet was placed inside a laser cutter (Full Spectrum Laser, NV, USA), and 3.3 x 15 mm rectangular inserts were cut out of the sheet. The power settings of the laser cutter were: raster power 1.1 %, raster speed 1.1 %, B/W threshold 165, and vector current 17 %. In addition to the fibrous scaffold inserts, flat polystyrene inserts were also cut to serve as a reference for current cell culture methods. The inserts were then carefully snapped off the polystyrene sheet, and eight inserts were placed in a 3.5 cm petri dish.

Insert sterilization and endothelial cell culture

The inserts were then washed with a 50 % ethanol solution and deionized water to remove any contamination and then placed in a vacuum chamber to dry overnight. Next, 1 mL of 0.3 mg/ml collagen (in 0.01 M HCl) was pipetted over the inserts and placed in a 37 °C environment until dried. Once the surface was coated with collagen, the inserts underwent standard sterilization procedures in a biohood consisting of spraying the surface with 70 % ethanol and air drying in UV.

Bovine pulmonary aortic endothelial cells (BPAECs, ATCC, VA, USA) with passage numbers 4-6 were used. DMEM media containing 10 % FBS and 1 % penicillin-streptomycin was used for culturing the cells. Post sterilization, 1 mL of BPAECs suspension (in DMEM media, 750,000 cells/mL) was pipetted onto the inserts in a petri dish. After 1 hour, an additional 1 mL of DMEM was added into each petri dish. Media

was changed every 24 hours. Cells were then cultured on the inserts until confluency, which was verified with an optical microscope. There were about 50,000 cells on each insert after confluency.

Device assembly and scaling up

The microfluidic system, providing biomimicry by introducing flow into a 3-dimensional cell culture model, consisted of 3 main parts: a peristaltic pump to provide flow, a microfluidic device designed to house the cell-inserts, and a reservoir to hold growth media. The microfluidic and reservoir devices were 3D-printed using a ProJet MJP 5600 system (3DSystems, SC, USA). External to the components mentioned above, the microfluidic system was connected by Tygon tubing (0.02" inner diameter, 0.06" mm outer diameter). The material for the 3D-printing was VisiJet® CR-CL 200, the exact composition of which is propriety, but is acrylate-based.

The microfluidic device consisted of three 3D-printed pieces, an enclosure designed to hold the inserts and form a microfluidic channel, and two adapters that could screw into each end of the enclosure. Modeled in Autodesk Inventor, the enclosure device was fabricated by extruding two slots through, with dimensions matching the inserts, to slide the inserts into the device with minimal effort. The slots were separated by a 300 μm spacer that developed into a microfluidic channel. On each end of the fluidic channel, a circular slot was designed to accommodate a commercially available O-ring for leakage-proof flows. At each end of the device, ports with standard 10x32 threading were incorporated so that the adapters could be easily screwed in. Tygon tubing (0.02" i.d.; 0.06" o.d.) was sealed through the 1.35 mm holes in the center of each adapter to connect the insert device.

Fig. 2 discerns the flow path of media throughout the device. First, cell-laden inserts were inserted into the insert device (**Figs. 2A & 2B**). Using the Tygon tubing, the circulatory flow path was built. Driven by a peristaltic pump, the media circulated through the tubing and into one end of the microfluidic device where media flowed over the cell-laden inserts to provide nutrients, any detection molecules/stimulants spiked into the media, and introduce shear stress. Media then exited the device and flowed to the reservoir (**Fig. 2C**). After the flow-based experiment, inserts were removed from the microfluidic device (**Fig. 2D**), and the cells were lysed to quantitate the number of cells on the inserts and analyze intracellular molecules of interest (**Fig. 2D**). The volume of the tubing and the fluidic channel in one flow was 500 μL , and thus, we added this much media at the beginning for each flow experiment.

Using a 12-channel peristaltic pump, 12 flow-based studies were conducted simultaneously. The reservoir device was designed to increase the modular functions of the system. The device was 3D printed

to contain 12 individual compartments, one for each flow channel. The top of the reservoir was fitted with a removable cap with two holes over each well. The smaller hole (800 μm diameter) was designed to accept the tubing coming from the microfluidic device, and the second (3.5 mm diameter hole) fit a standard 12-channel pipette for simultaneous sampling from or adding reagents to the flow channels.

Characterization of cell morphologies on flat and on the aligned fibers

Cell inserts were fixed in methanol for 10 min in a $-20\text{ }^{\circ}\text{C}$ environment and then stained with a 0.5 % (w/v) crystal violet solution in 25 % (v/v) methanol to analyze the aspect ratios of the cells in ImageJ, a free image processing program. The alignment of the cells was also determined through observation of the angle of the cell elongation path (length) against the direction of the fibers. A live/dead staining kit (Thermo Fisher Scientific, MA, USA) was used along with fluorescent imaging to detect viability.

NO release measurement

The release of nitric oxide (NO) from BPAECs on the fibrous topography was compared to that from cells on a flat surface. The 12 flow experiments were divided into 3 groups: 4 channels contained inserts without cells to serve as analytical blanks; 4 channels contained cells cultured on flat inserts; and 4 channels had cells on the aligned fibrous scaffold. A total of 10 mL DMEM media (without phenol red) was supplemented DAF-FM and ATP to final concentrations of 5 μM and 10 μM , respectively. Two confluent cell-laden inserts of each condition were carefully placed in each microfluidic device with the cells contacting the flow channel. Then, 400 μL of the spiked DMEM was pipetted into each well in the reservoir device. The whole setup was placed in an incubator ($37\text{ }^{\circ}\text{C}$, 5% CO_2 , humid) at a flow rate of 1.5 mL/min for 2 hours.

After 2 hours, 150 μL of the DMEM was pipetted out of the reservoir device and loaded into a 96 well plate. Next, the fluorescence emission of DAF-FM was measured (ex. 485 nm; em. 520 nm). Concurrently, the inserts were quickly removed from the microfluidic devices and washed thoroughly with 10mM HEPES buffer, followed by lysis in 400 μL RIPA buffer using an ultrasonic homogenizer for 1 min. The protein amount in each lysate was measured by the BCA assay as a measurement of cell numbers for data normalization.

A standard curve was created to determine the NO concentration present in the media. A PBS solution was degassed first with argon gas to remove any lingering oxygen, and then saturated with compressed NO gas to reach a final concentration of 1.9 mM. Then in degassed PBS, a series of NO dilutions (0, 0.625, 1.25, 5, and 10 μM) were made and reacted with DAF-FM in a nitrogenous environment,

followed by fluorescence detection. Fig. S4 in the supplementary information shows a calibration curve made this way, with the detection limit being 0.26 μM .

Intracellular metabolomics measurements (arginine, citrulline, and ornithine)

An aliquot of 200 μL of LCMS grade water with 4 μM ^{13}C -phenylalanine (internal standard for LCMS analyses) was added to each lysate vial. Cell lysates were then lyophilized and reconstituted in LCMS grade isopropanol to precipitate excess salts and proteins. Then samples were then centrifuged at 14,000 rpm (Eppendorf, Centrifuge 5424R, NY, USA) at 4 $^{\circ}\text{C}$ for 15 min. The supernatant was transferred to another clean vial, followed by lyophilization. Finally, the dry extracts were reconstituted in 15 μL LCMS grade water with 0.1% formic acid and transferred to LC-MS instrument³⁰.

The Agilent G6530C LC QTOF system equipped with the capillary HPLC 1260 Infinity series were used for the analyses. For both positive detection mode, a full scan range of 50 to 1000 m/z with a mass accuracy of 2 ppm was performed. For the positive mode, ESI ion source parameters were: gas temperature 320 $^{\circ}\text{C}$, drying gas 10 L/min, nebulizer 30 psi, and capillary voltage 3500 V. The fragmentor, skimmer, and OCT1 RF Vpp were set to 110, 65 and 750 volts, respectively.

A C18 column (Luna[®] Omega 1.6 μm , PS 100 \AA with an inner diameter of 100 \times 2.1 mm, Phenomenex, CA, USA) was used with the following gradient: mobile phase A was 0.1 % formic acid in water; mobile phase B was LC-MS grade methanol. At positive mode, the gradient started with 100% A at 0 min, and decreased to 0% A at 15 min. The A phase was remained at 0% till 25 min, followed by being increased to 100% at 30 min and held until 45 min. The flow rate was set at 30 $\mu\text{L}/\text{min}$. An aliquot of 5 μL of samples was injected into the column by an autosampler for each run.

Peak areas of arginine, ornithine and citrulline were analyzed by MassHunter Qualitative Analysis Version B.10, which were then normalized to the internal standard (^{13}C -Phenylalanine) and then the cell number obtained from the protein assay.

eNOS activity probing

The activity of the eNOS in each ECM condition was quantitated by a commercially available assay kit (Abcam, Cambridge, UK). The cells were washed and lysed according to the user manual. The substrate molecule in the kit could be converted by eNOS in the cell lysates to a fluorescent product, based on which, the activity of eNOS could be quantitated.

Data normalization

For each measurement above (NO, metabolites, eNOS), all quantified results were normalized by cell numbers. Specifically, the cells in each fluidic device (2 inserts) were lysed in 500 μ L RIPA buffer, followed by total protein quantitation using the BCA assay (ThermoFisher, PA, USA). A calibration curve was made by lysing various known numbers of cells (counted on a hemocytometer) and quantitating the protein content (BCA assay) in each lysate.

Statistics

Replicate numbers were indicated in the captions of the data figures. We applied the two-sample t-test for significance determination, except for the normalized eNOS activity data, where a one-sample t-test was performed. Significant differences were valid only when p values were smaller than 0.05.

RESULTS AND DISCUSSION

Current dynamic endothelial models applied the cells on a 2D flat surface—either a wall of a microchannel, the bottom of a reservoir, or a sealed porous membrane. However, some recent studies have shown that the biophysical cues of an ECM can affect cellular activities^{13, 31-33}. Therefore, we hypothesized that the aligned fibrous topography (**Fig. 1**) on native endothelial ECM could affect the functions of endothelial cells. However, with PDMS (polydimethylsiloxane)-based microfluidic technology, the incorporation of additional microstructures (e.g., fibrous ECMs) will significantly increase the difficulty of fabrication and maintenance. Therefore, we developed a new microfluidic system with easy ECM inclusion, which was also robust enough

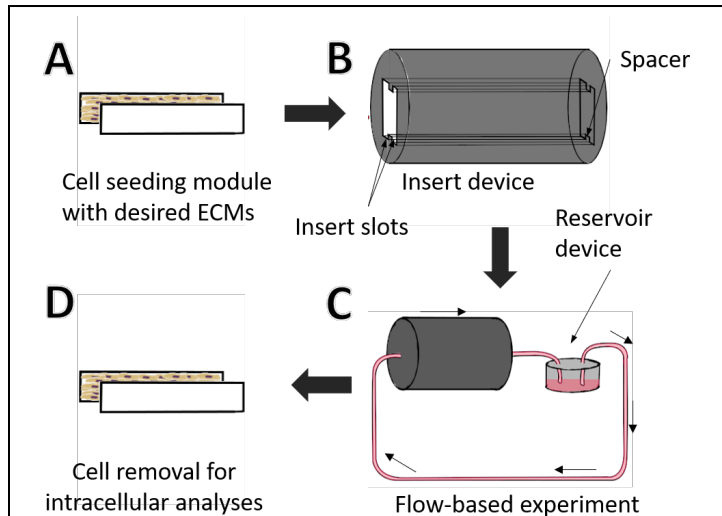
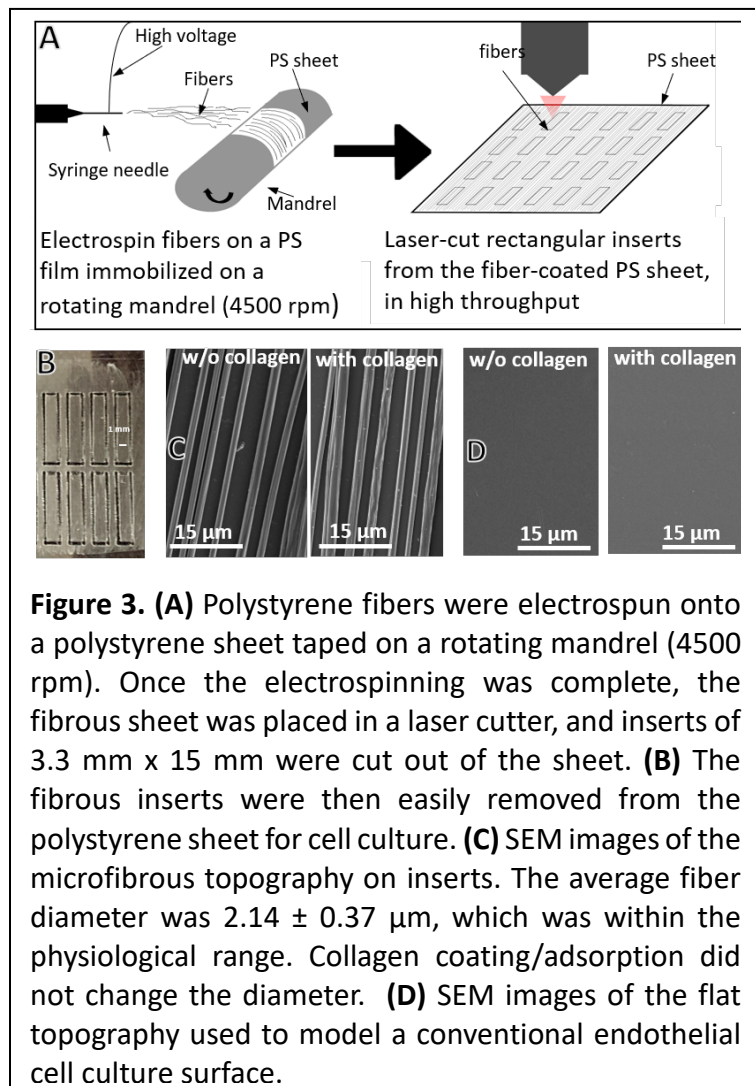


Figure 2. Overview of the microfluidic system. **(A)** ECMs of desired topographies were fabricated on rectangular inserts, where cells were seeded. **(B)** The device where the inserts could be assembled to form a microfluidic channel. **(C)** After the device was assembled, tubing was connected to both ends for media to circulate via a reservoir device. **(D)** After a flow-based study, the cell-laden inserts were removed for further investigations of intracellular metabolites.

to perform simultaneous parallel experiments.

Fig. 2 overviews the general concept of the microfluidic design. First, instead of incorporating ECMs in a fully integrated microfluidic device, ECMs of desired topographies were prepared separately as rectangular inserts, where endothelial cells were seeded. A microfluidic device was 3D-printed with slots that fit the cell-laden inserts. 3D-printing has emerged as a powerful tool to fabricate robust and standardized microfluidic devices with intricate inner microstructures^{32, 34, 35}. During a flow-based experiment, stimulants could be added, and samples could be taken via the openings on top of the reservoir. After a study, the cell inserts could be removed for further analyses such as lysate extraction. This microfluidic technology has several advantages: 1) the modularity allowed for a failed module to be quickly replaced without sacrificing the whole setup; 2) the quality of cell cultures (e.g., contamination) could be checked before a flow study to ensure reliable cell assays; 3) the prepared culture surface could be easily manipulated to simulate different ECM topographies, e.g., allowing users to study cellular functions on a damaged and healthy ECM concurrently. The design, characterization, and performance of each part of the system are thoroughly discussed below.

The cell-laden inserts with desired ECMs



We applied electrospinning to produce microfibers to mimic the aligned fibrous topography of the native basement membrane. Electrospinning is a technique that uses a high voltage (typically on a syringe needle) to convert a polymer solution into fibers³⁶⁻³⁸. By varying the concentration of the polymer solution, the delivery rate, the syringe needle size, and the voltage, the fiber size is tunable. As shown in

Fig. 3A, we pumped a polystyrene (PS) solution at 1.5 mL/hr through a 20-gauge blunt syringe needle connected to a 22.5 kV power supply. By collecting the generated fibers on a polystyrene sheet taped on a steel rotating mandrel (4500 rpm), a single layer of aligned microfibers was obtained. Next, the fiber-coated PS sheet was laser cut into rectangular inserts. The PS sheet was used as a rigid support structure to immobilize the flexible fibers. These fibrous inserts could be prepared in high throughput. **Fig. 3B** demonstrates a small portion of an array of inserts prepared at a time. The material polystyrene was chosen because of its biocompatibility³⁹. With this protocol, aligned fibers with an average diameter of $2.14 \pm 0.37 \mu\text{m}$, which was within the physiological range of conduit arteries (**Fig. 1**; 1-3 μm) were generated (**Fig. 3C**). We also prepared inserts with a flat topography (**Fig. 3D**) for control experiments. All the inserts were coated with collagen before endothelial cell culturing.

The laser cutting process served two critical functions in the 3D scaffold manufacturing process: 1) it ensured the surface area of the insert was consistent, and 2) as the edges were cut, the fibers were fused onto the surface of the polystyrene support. To avoid the shrinkage associated with excess heat to the polystyrene sheet, the edges of the inserts were etched into the sheet so that they could easily be snapped off by tweezers. This ensured the accuracy of the insert dimensions.

The microfluidic device

The microfluidic device was 3D-printed in a cylindrical shape with threaded ports and O-ring notches at both ends, and a channel through (**Figs. 4A** and **4B**). Design details of the pieces can be found in the SI. **Fig. 4C** shows an assembled device after O-rings and the rectangular inserts were integrated. As shown in **Fig. 4D**, the two inserts were

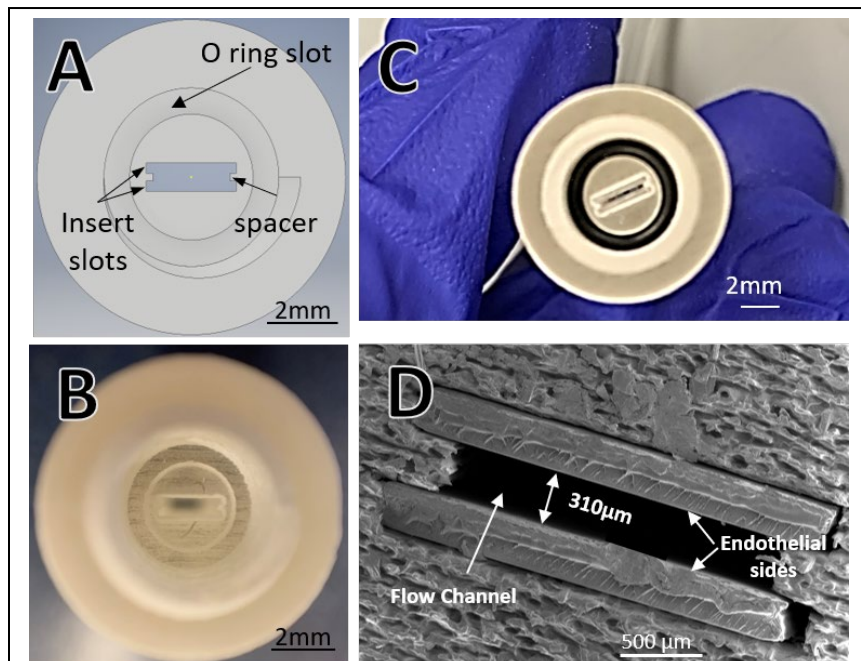


Figure 4. (A) Cross view of the CAD design of the microfluidic device. (B) The actual view of the printed device. (C) An assembled device with inserts and O-ring. (D) An SEM image of the cross-view of an assembled device. The two inserts were secured firmly with a microfluidic channel of 310 μm formed in between.

secured tightly in the slots with a fluidic channel of 310 μm formed in between. Standard 10 x 32 threads were 3D-printed along with the threaded ports on the devices, where customized (**Fig. 5A**) or commercially available fittings could be applied to connect tubing for flow-based investigations. With the robustness of the device (hard material), the inclusion of O-rings, and the standardized threads, we could flow media at high rates up to 4,000 $\mu\text{L}/\text{min}$ without leakage, which covered the whole physiological shear stress range in human blood vessels (0-80 dyne/cm^2). This wide adoptability of shear stress on our device is critically important for endothelial studies especially when modeling diseases with modified shear

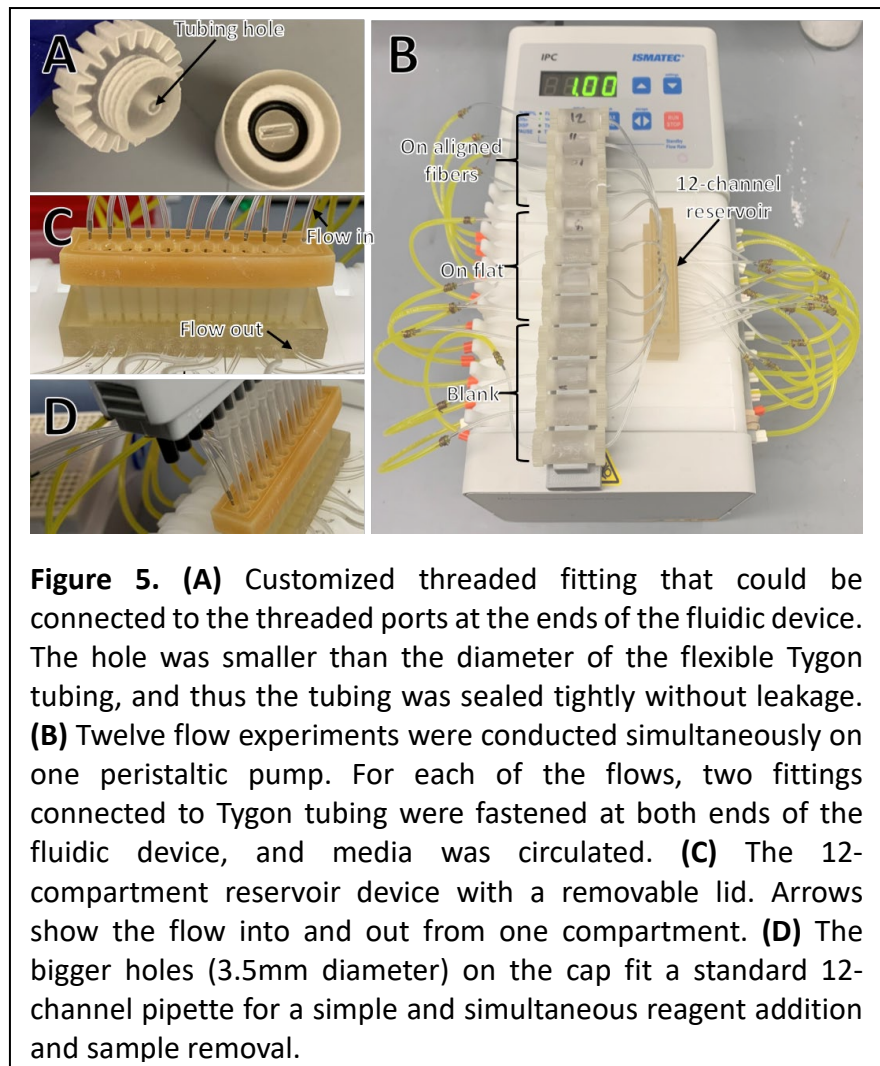


Figure 5. (A) Customized threaded fitting that could be connected to the threaded ports at the ends of the fluidic device. The hole was smaller than the diameter of the flexible Tygon tubing, and thus the tubing was sealed tightly without leakage. (B) Twelve flow experiments were conducted simultaneously on one peristaltic pump. For each of the flows, two fittings connected to Tygon tubing were fastened at both ends of the fluidic device, and media was circulated. (C) The 12-compartment reservoir device with a removable lid. Arrows show the flow into and out from one compartment. (D) The bigger holes (3.5mm diameter) on the cap fit a standard 12-channel pipette for a simple and simultaneous reagent addition and sample removal.

stress (e.g., hypertension). There has not been a microfluidic device that could handle such high flow rates/shear stress.

Throughput enhancement

Compared to static cell cultures in a multi-well plate, a drawback of conventional microfluidics is the low throughput (typically one device per experiment), which is likely caused by the high facility and personnel requirements to fabricate and maintain the devices. With 3D-printing, however, robust devices of the same geometry can be massively produced, making it possible to scale up parallelized studies. As shown in **Fig. 5B**, on a multi-channel peristaltic pump, we set up 12 flow experiments conducted

simultaneously to improve throughput. Moreover, studying various treatments on cells under the same environment helped reduce result variances. We also created a reservoir device as an interfacing window for the studies, which contained 12 compartments for each of the flows (**Fig. 5C**). This device acted as a transfer station for the flowing media—using a 12-channel pipette, molecules (e.g., fluorescent probes) can be added, and samples can be taken at the same time with ease (**Fig. 5D**). All the 3D-printed parts were reusable after being bleached, rinsed, and autoclaved. The number of parallel experiments was only limited by the available slots on the peristaltic pump (in our case 12); however, with a larger pump (24 and 36 channels are commercially available), more flow channels can be tested.

The role of the aligned fibrous topography on endothelial cells

We cultured endothelial cells on inserts with aligned fibers or a flat surface and found that the topographic cue could guide cell morphology. As shown in **Fig. S5** in the SI, endothelial cells were organized along the fibers with enhanced aspect ratios, while both surfaces supported cell viability. Next, the cell-laden inserts (with fibers or flat) were integrated into the 3D-printed microfluidic device (**Fig. 5A**) and scaled up (**Fig. 5B**) for flow-based explorations. A flow rate of 1.5 mL/min with the corresponding shear stress of 7.8 dyne/cm² was applied to mimic the conduit arteries *in vivo*,

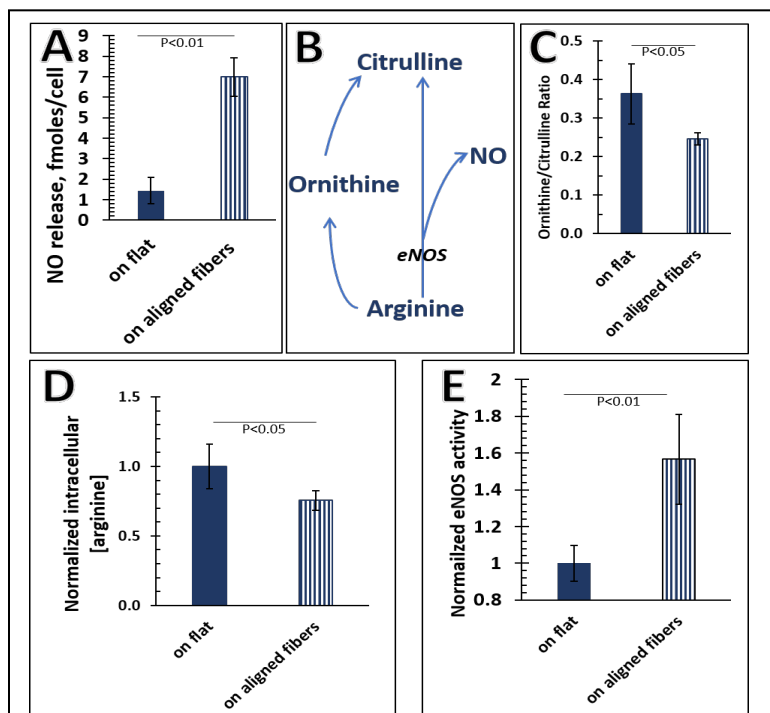


Figure 6. (A) Cells cultured on the fibrous scaffold exhibited a 4.88-fold ($P<0.01$) increase in NO released than those grown on a flat surface ($N=10$, error=S.E.M.). **(B)** The arginine pathway in endothelial cells that produces citrulline either by eNOS that generates NO, or through ornithine without NO production. **(C)** LC-MS quantitation revealed that the ornithine/citrulline ratio was significantly higher (by 1.5 fold, $p<0.05$) in cells cultured on flat than those on the aligned fibers, indicating more arginine was metabolized via the ornithine pathway ($N=15$, error=S.E.M.). **(D)** LC-MS results showed less (by 1.3 fold) intracellular arginine in cells on the aligned fibers vs. cells on flat ($N=15$, error=S.E.M.). **(E)** Cells on the fibers demonstrated a significantly higher (by 1.6 fold, $p<0.05$) eNOS activity than cells cultured on the flat surface ($N=4$, error=S.E.M.).

which is the main site for the pathogenesis of endothelial cell-involved CVDs^{40, 41}. We investigated the release of nitric oxide (NO) from endothelial cells, one of the most important signaling molecules produced by the cells to maintain the homeostasis of blood and surrounding tissues. To measure the levels of extra cellular NO, we spiked into each flow chamber via the reservoir device (**Fig. 5C**) the DAF-FM solution, a commonly used fluorescent probe for extracellular NO—after binding specifically to NO, the quantum yield of the probe is significantly increased with bright fluorescent emission at 520 nm⁴². Compared to its diacetate derivative (DAF-FM-DA), which can polarize cell membranes, the DAF-FM cannot diffuse into cells. The circulating media (with DAF-FM) was collected from the reservoir device after 2 hr, followed by fluorescence measurements. As shown in **Fig. 6A**, endothelial cells cultured on the aligned fibrous topography released significantly more NO than those on the flat surface. Because NO is produced intracellularly by arginine breakdown to citrulline, which can also be metabolized via an alternative way through ornithine (**Fig. 6B**), we took the cell-laden inserts out of the fluidic devices, lysed the cells immediately, and detected the three amino acids in the lysates using LC-MS. **Fig. 6C** demonstrates that the ornithine/citrulline ratio in cells cultured on flat was higher than cells on the fibers, suggesting more alternative arginine metabolism occurred, thus decreasing NO⁴³. The levels of arginine, the biological precursor of NO was also found to be lower in the cells on fiber (**Fig. 6D**), which is consistent with higher arginine conversion rates in the cells on fiber. Subsequent evaluation of endothelial nitric oxide synthase (eNOS) revealed that this enzyme was more active in cells on the fibers, which explained the lower arginine level. Collectively, these data strongly demonstrated that the aligned fibrous topography on the ECM altered NO release from endothelial cells by increasing the overall metabolism of arginine to NO and thereby reducing its diversion to the ornithine metabolism route.

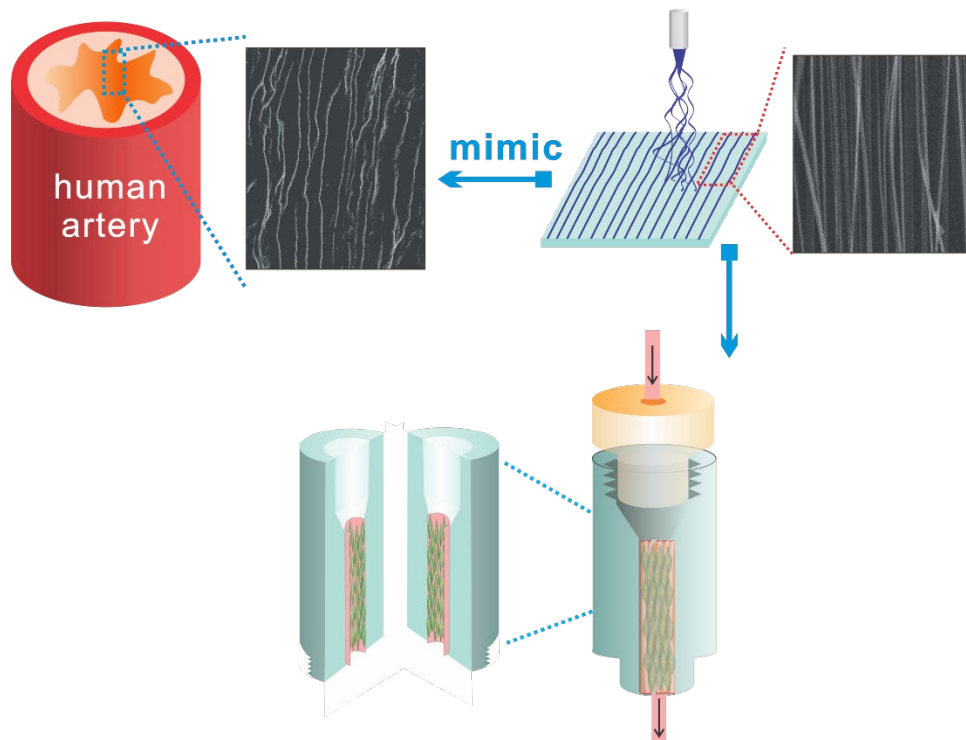
CONCLUSION

In this paper, we present a modular microfluidic-based endothelial model fabricated by 3D-printing and electrospinning, which enabled integration of desired ECM topographies, physiologically relevant shear stress, and cellular analyses in a parallel manner. There has not been an endothelial model like this. We also included the design details of the devices in the SI to promote technology translation. By mimicking the microstructure on the inner wall of human arteries, we found that the aligned fibrous topography enhanced endothelial cell-derived NO production via controlling arginine metabolism pathways. This is first time to include the physiologically-relevant ECM topography for endothelial cells in a microfluidic device, and to report the effects of the ECM on endothelial functions. These results

enhanced our understanding of endothelial biology, and indicated the necessity to consider relevant surface topography in future endothelial modeling.

Supporting information. The electrospinner setup; Engineering sketches of the 3D-printed devices; a NO calibration curve; Cell morphology analyses

For Table of Contents Use Only



REFERENCES

1. Ramnath, R. D.; Satchell, S. C., Glomerular Endothelial Cells: Assessment of Barrier Properties In Vitro. In *Diabetic Nephropathy: Methods and Protocols*, Gnudi, L.; Long, D. A., Eds. Springer US: New York, NY, 2020; pp 145-151.
2. Rajendran, P.; Rengarajan, T.; Thangavel, J.; Nishigaki, Y.; Sakthisekaran, D.; Sethi, G.; Nishigaki, I., The vascular endothelium and human diseases. *International journal of biological sciences* **2013**, *9* (10), 1057-1069.
3. Wang Julie, C.; Bennett, M., Aging and Atherosclerosis. *Circulation Research* **2012**, *111* (2), 245-259.
4. Hadi, H. A. R.; Carr, C. S.; Al Suwaidi, J., Endothelial dysfunction: cardiovascular risk factors, therapy, and outcome. *Vascular health and risk management* **2005**, *1* (3), 183-198.
5. Giannitsi, S.; Bougiakli, M.; Bechlioulis, A.; Naka, K., Endothelial dysfunction and heart failure: A review of the existing bibliography with emphasis on flow mediated dilation. *JRSM cardiovascular disease* **2019**, *8*, 2048004019843047-2048004019843047.
6. Dimmeler, S.; Zeiher Andreas, M., Endothelial Cell Apoptosis in Angiogenesis and Vessel Regression. *Circulation Research* **2000**, *87* (6), 434-439.
7. Tan, W.; Desai, T. A., Layer-by-layer microfluidics for biomimetic three-dimensional structures. *Biomaterials* **2004**, *25* (7), 1355-1364.
8. Jia, L.; Han, F.; Yang, H.; Turnbull, G.; Wang, J.; Clarke, J.; Shu, W.; Guo, M.; Li, B., Microfluidic Fabrication of Biomimetic Helical Hydrogel Microfibers for Blood-Vessel-on-a-Chip Applications. *Advanced Healthcare Materials* **2019**, *8* (13), 1900435.
9. van der Meer, A. D.; Poot, A. A.; Feijen, J.; Vermes, I., Analyzing shear stress-induced alignment of actin filaments in endothelial cells with a microfluidic assay. *Biomicrofluidics* **2010**, *4* (1), 11103-11103.
10. Thoumine, O.; Nerem, R. M.; Girard, P. R., Changes in organization and composition of the extracellular matrix underlying cultured endothelial cells exposed to laminar steady shear stress. *Laboratory investigation; a journal of technical methods and pathology* **1995**, *73* (4), 565-576.
11. Lee, D. W.; Choi, N.; Sung, J. H., A microfluidic chip with gravity-induced unidirectional flow for perfusion cell culture. *Biotechnol Prog* **2019**, *35* (1), e2701.
12. Chen, Z. Z.; Yuan, W. M.; Xiang, C.; Zeng, D. P.; Liu, B.; Qin, K. R., A microfluidic device with spatiotemporal wall shear stress and ATP signals to investigate the intracellular calcium dynamics in vascular endothelial cells. *Biomech Model Mechanobiol* **2019**, *18* (1), 189-202.
13. Munshi, A. S.; Chen, C.; Townsend, A. D.; Martin, R. S., Use of 3D Printing and Modular Microfluidics to Integrate Cell Culture, Injections and Electrochemical Analysis. *Analytical methods : advancing methods and applications* **2018**, *10* (27), 3364-3374.
14. Sasaki, N.; Hayashi, T.; Inoue, N.; Onishi, M., Fabrication of Microfluidic Cell Culture Devices Using a Consumer Laser Cutter. *BUNSEKI KAGAKU* **2018**, *67* (7), 379-386.
15. van der Helm, M. W.; Odijk, M.; Frimat, J. P.; van der Meer, A. D.; Eijkel, J. C. T.; van den Berg, A.; Segerink, L. I., Direct quantification of transendothelial electrical resistance in organs-on-chips. *Biosens Bioelectron* **2016**, *85*, 924-929.
16. Xu, H.; Li, Z.; Guo, Y.; Peng, X.; Qin, J., Probing the response of lung tumor cells to inflammatory microvascular endothelial cells on fluidic microdevice. *ELECTROPHORESIS* **2017**, *38* (2), 311-319.
17. Wu, S. Y.; Hou, H. S.; Sun, Y. S.; Cheng, J. Y.; Lo, K. Y., Correlation between cell migration and reactive oxygen species under electric field stimulation. *Biomicrofluidics* **2015**, *9* (5), 054120.
18. Cahill, P. A.; Redmond, E. M., Vascular endothelium – Gatekeeper of vessel health. *Atherosclerosis* **2016**, *248*, 97-109.

19. Klee, D.; Höcker, H., Polymers for Biomedical Applications: Improvement of the Interface Compatibility. In *Biomedical Applications Polymer Blends*, Eastmond, G. C.; Höcker, H.; Klee, D., Eds. Springer Berlin Heidelberg: Berlin, Heidelberg, 1999; pp 1-57.
20. Dickinson, L. E.; Rand, D. R.; Tsao, J.; Eberle, W.; Gerecht, S., Endothelial cell responses to micropillar substrates of varying dimensions and stiffness. *Journal of biomedical materials research. Part A* **2012**, *100* (6), 1457-1466.
21. Dye, J. F.; Lawrence, L.; Linge, C.; Leach, L.; Firth, J. A.; Clark, P., Distinct Patterns of Microvascular Endothelial Cell Morphology Are Determined by Extracellular Matrix Composition. *Endothelium* **2004**, *11* (3-4), 151-167.
22. Anderson, D. E. J.; Hinds, M. T., Extracellular matrix production and regulation in micropatterned endothelial cells. *Biochemical and Biophysical Research Communications* **2012**, *427* (1), 159-164.
23. Ballermann, B. J.; Dardik, A.; Eng, E.; Liu, A., Shear stress and the endothelium. *Kidney International* **1998**, *54*, S100-S108.
24. Archer, S. L.; Huang, J. M.; Hampl, V.; Nelson, D. P.; Shultz, P. J.; Weir, E. K., Nitric oxide and cGMP cause vasorelaxation by activation of a charybdotoxin-sensitive K channel by cGMP-dependent protein kinase. *Proceedings of the National Academy of Sciences of the United States of America* **1994**, *91* (16), 7583-7587.
25. de Souza, M. d. G. C.; Bouskela, E., Arteriolar diameter and spontaneous vasomotion: Importance of potassium channels and nitric oxide. *Microvascular Research* **2013**, *90*, 121-127.
26. Kubes, P.; Suzuki, M.; Granger, D. N., Nitric oxide: an endogenous modulator of leukocyte adhesion. *Proceedings of the National Academy of Sciences* **1991**, *88* (11), 4651.
27. Moncada, S.; Palmer, R. M.; Higgs, E. A., Nitric oxide: physiology, pathophysiology, and pharmacology. *Pharmacological Reviews* **1991**, *43* (2), 109.
28. Moncada, S.; Higgs, A., The L-Arginine-Nitric Oxide Pathway. *New England Journal of Medicine* **1993**, *329* (27), 2002-2012.
29. Huang, T. J.; Armbruster, M. R.; Coulton, J. B.; Edwards, J. L., Chemical Tagging in Mass Spectrometry for Systems Biology. *Anal Chem* **2019**, *91* (1), 109-125.
30. Huang, T. J.; Armbruster, M.; Lee, R.; Hui, D. S.; Edwards, J. L., Metabolomic analysis of mammalian cells and human tissue through one-pot two stage derivatizations using sheathless capillary electrophoresis-electrospray ionization-mass spectrometry. *J Chromatogr A* **2018**, *1567*, 219-225.
31. Chen, T. T.; Luque, A.; Lee, S.; Anderson, S. M.; Segura, T.; Iruela-Arispe, M. L., Anchorage of VEGF to the extracellular matrix conveys differential signaling responses to endothelial cells. *The Journal of Cell Biology* **2010**, *188* (4), 595-609.
32. Chen, C.; Townsend, A. D.; Hayter, E. A.; Birk, H. M.; Sell, S. A.; Martin, R. S., Insert-based microfluidics for 3D cell culture with analysis. *Analytical and Bioanalytical Chemistry* **2018**, *410* (12), 3025-3035.
33. Song, K. H.; Heo, S.-J.; Peredo, A. P.; Davidson, M. D.; Mauck, R. L.; Burdick, J. A., Influence of Fiber Stiffness on Meniscal Cell Migration into Dense Fibrous Networks. *Advanced Healthcare Materials* **2019**, *n/a* (n/a), 1901228.
34. Chen, C.; Mehl, B. T.; Sell, S. A.; Martin, R. S., Use of electrospinning and dynamic air focusing to create three-dimensional cell culture scaffolds in microfluidic devices. *The Analyst* **2016**, *141* (18), 5311-5320.
35. Chen, C.; Townsend, A. D.; Sell, S. A.; Martin, R. S., Microchip-based 3D-cell culture using polymer nanofibers generated by solution blow spinning. *Analytical Methods* **2017**, *9* (22), 3274-3283.
36. Bhardwaj, N.; Kundu, S. C., Electrospinning: A fascinating fiber fabrication technique. *Biotechnology Advances* **2010**, *28* (3), 325-347.
37. Schiffman, J. D.; Schauer, C. L., A Review: Electrospinning of Biopolymer Nanofibers and their Applications. *Polymer Reviews* **2008**, *48* (2), 317-352.

38. Kevin, P. F.; Emily, A. G. K.; Chengpeng, C.; Martin, R. S.; Scott, A. S., A review of electrospinning manipulation techniques to direct fiber deposition and maximize pore size. *Electrospinning* **2017**, 2 (1), 46-61.
39. Lerman, M. J.; Lembong, J.; Muramoto, S.; Gillen, G.; Fisher, J. P., The Evolution of Polystyrene as a Cell Culture Material. *Tissue engineering. Part B, Reviews* **2018**, 24 (5), 359-372.
40. Reneman, R. S.; Hoeks, A. P. G., Wall shear stress as measured in vivo: consequences for the design of the arterial system. *Medical & biological engineering & computing* **2008**, 46 (5), 499-507.
41. Zhang, X.; Yao, Z. Q.; Karuna, T.; He, X. Y.; Wang, X. M.; Li, X. F.; Liu, W. C.; Li, R.; Guo, S. Q.; Chen, Y. C.; Li, G. C.; Duan, C. Z., The role of wall shear stress in the parent artery as an independent variable in the formation status of anterior communicating artery aneurysms. *Eur Radiol* **2019**, 29 (2), 689-698.
42. Namin, S. M.; Nofallah, S.; Joshi, M. S.; Kavallieratos, K.; Tsoukias, N. M., Kinetic analysis of DAF-FM activation by NO: toward calibration of a NO-sensitive fluorescent dye. *Nitric oxide : biology and chemistry* **2013**, 28, 39-46.
43. Kovamees, O.; Shemyakin, A.; Pernow, J., Amino acid metabolism reflecting arginase activity is increased in patients with type 2 diabetes and associated with endothelial dysfunction. *Diabetes Vasc Dis Re* **2016**, 13 (5), 354-360.